

1**Second Sound in Ultracold Atomic Gases**Lev Pitaevskii^a and Sandro Stringari^b**Abstract**

We provide an overview of the recent theoretical and experimental advances in the study of second sound in ultracold atomic gases. Starting from the Landau's two fluid hydrodynamic equations we develop the theory of first and second sound in various configurations characterized by different geometries and quantum statistics. These include the weakly interacting 3D Bose gas, the strongly interacting Fermi gas at unitarity in the presence of highly elongated traps and the dilute 2D Bose gas, characterized by the Berezinsky-Kosterlitz-Thouless transition. An explicit comparison with the propagation of second sound in liquid Helium is carried out to elucidate the main analogies and differences. We also make an explicit comparison with the available experimental data and point out the crucial role played by the superfluid density in determining the temperature dependence of the second sound speed.

1.1 Introduction

Superfluidity is one of the most challenging features characterizing the behavior of ultra cold atomic gases and provides an important interdisciplinary connection with the physics of other many-body systems both in condensed matter (superfluid Helium, superconductivity) and high energy physics (nuclear superfluidity, neutron stars). It is a phenomenon deeply related to

^a INO-CNR BEC Center and Dipartimento di Fisica, Università di Trento, Via Sommarive 14, I-38123 Povo, Italy; Kapitza Institute for Physical Problems, RAS, ul Kosygina 2, 119334 Moscow, Russia

^b INO-CNR BEC Center and Dipartimento di Fisica, Università di Trento, Via Sommarive 14, I-38123 Povo, Italy

Bose-Einstein condensation, which, in the case of Fermi superfluids, corresponds to the condensation of pairs. Several manifestations of superfluidity have already emerged in experiments on ultracold atomic gases, either in the case of bosons and fermions [49].

Important phenomena are the consequence of the irrotational nature of the velocity field associated with the superfluid flow. They include the occurrence of quantized vortices, which is actually a direct manifestation of the absence of shear viscosity, the quenching of the moment of inertia, and the behavior of the collective oscillations at zero temperature. Vortices in a superfluid are characterized by the quantization of the circulation $\oint \mathbf{v}_s \cdot d\mathbf{l}$ of the superfluid velocity around the vortex line. They have become experimentally available using different approaches. A first procedure consists of creating the vortical configuration with optical methods in two-component condensates [37]. A second method, which shares a closer resemblance with the rotating bucket experiment of superfluid helium, makes use of a suitable rotating modulation of the trap to stir the condensate [35]. Above a critical angular velocity one observes the formation of vortices which are imaged after expansion. Configurations containing a large number of vortices can be created by stirring the condensate at angular velocities close to the centrifugal limit and have been realized in both Bose [1, 12], and Fermi [66] superfluid gases. The quenching of the moment of inertia due to superfluidity shows up in the peculiar behavior of the scissors mode [19, 36] and its temperature dependence has been detected directly by measuring the angular momentum of a trapped superfluid rotating at a given angular velocity [53]. The effects of irrotationality on the collective oscillations of both Bose and Fermi superfluid gases have been the object of extensive theoretical and experimental work, and are accurately described by superfluid hydrodynamics in the presence of harmonic traps [56].

An important consequence of superfluidity is the occurrence of a critical velocity below which the superfluid can move without dissipation (Landau's criterion). These experiments were carried out with moving focused laser beams ([43]) as well as with moving one-dimensional optical lattices [40]. Other manifestations of superfluidity are provided by the coherent macroscopic behavior responsible for quantum tunneling in the double well geometry [3] and, in the case of Fermi superfluids, by the appearance of a gap in the single-particle excitation spectrum, revealed by radio frequency transitions [11]. Let us also mention the recent experimental investigation of the equation of state of a strongly interacting Fermi gas [30]. This measurement has revealed the typical λ -behavior of the specific heat at the superfluid transition and an accurate determination of the critical temperature.

A key property of a superfluid at finite temperature is its two-fluid nature, i.e. the simultaneous presence of two flows: a dissipationless superfluid flow and a normal flow. The propagation of second sound [15], which represents the topic of discussion of the present work, is a direct manifestation of this two-fluid nature. An important feature of second sound is that it can provide unique information on the temperature dependence of the superfluid density, as proven in the case of superfluid helium. For this reason its investigation permits to better clarify the conceptual difference between superfluidity and Bose-Einstein condensation. This distinction is particularly important in strongly interacting gases (like the Fermi gas at unitarity) and it is even more dramatic in two dimensions where long range order, yielding Bose-Einstein condensation, is ruled out at finite temperature by the Hohenberg-Mermin-Wagner theorem.

In this paper we summarize some advances in the understanding of second sound in quantum gases that have been achieved theoretically and experimentally in the last few years. In Section 2 we discuss the general behavior of the Landau's equations of two fluid hydrodynamics. In Section 3 we discuss the solutions of these equations in the case of a 3D dilute Bose gas. In Section 4 we apply the equations to the case of a Fermi gas at unitarity in the presence of tight radial trapping conditions giving rise to highly elongated configurations which are suitable for the experimental investigation of sound waves. Finally in Section 5 we discuss the behavior of second sound in 2D Bose gases where its measurement could provide unique information on the behavior of the superfluid density.

1.2 Two-fluid hydrodynamics: first and second sound

In the present work we will describe the macroscopic dynamic behavior of a superfluid at finite temperature. We will consider situations where the free path of the elementary excitation is small compared to the wavelength of the sound wave and local thermodynamic equilibrium is ensured by collisions. This condition is rather severe at low temperature where collisions are rare. It permits to define locally (in space and time) the thermodynamic properties of the fluid, like the temperature, the pressure etc.. The general system of equations describing the macroscopic dynamic behavior of the superfluid at finite temperature was obtained by Landau [31] (see also Ref. [32]).

In the following we will limit ourselves to the description of small velocities and small amplitude oscillations, corresponding to the linearized solutions of the equations of motion. The propagation of such oscillations at finite

temperature provides an important tool to investigate the consequences of superfluidity. The equation for the superfluid velocity \mathbf{v}_s obeys the fundamental irrotational form

$$m \frac{\partial \mathbf{v}_s}{\partial t} + \nabla(\mu + V_{ext}) = 0 \quad (1.1)$$

fixed by the chemical potential $\mu(\rho, T)$ of uniform matter which, in general, depends on the local value of the density and of the temperature.

The equation for the density n has the usual form of the continuity equation:

$$\frac{\partial n}{\partial t} + \text{div} \mathbf{j} = 0. \quad (1.2)$$

where the current density \mathbf{j} can be separated into the normal and superfluid components $\mathbf{j} = n_s \mathbf{v}_s + n_n \mathbf{v}_n$ with $n_s + n_n = n$. The time derivative of the current density is equal to the force per unit volume which, in the linear approximation, is fixed by the gradient of the pressure and by the external potential (Euler equation):

$$\frac{\partial \mathbf{j}}{\partial t} + \frac{\nabla P}{m} + \frac{n}{m} \nabla V_{ext} = 0. \quad (1.3)$$

The last equation is the equation for the entropy density s . This can be derived from general arguments. In fact if dissipative processes such as viscosity and thermoconductivity are absent, the entropy is conserved and the equation for s takes the form of a continuity equation. Furthermore only elementary excitations contribute to the entropy whose transport is hence fixed by the normal velocity \mathbf{v}_n of the fluid. The equation for the entropy then takes the form

$$\frac{\partial s}{\partial t} + \text{div}(s \mathbf{v}_n) = 0 \quad (1.4)$$

where, in the linear regime, the entropy entering the second term should be calculated at equilibrium.

The thermodynamic quantities entering the above equations are not independent and obey the Gibbs-Duhem thermodynamic equation $n d\mu = -s dT + dP$. It is worth mentioning that also this thermodynamic identity is valid only in the linear regime. In fact in general the thermodynamic functions can exhibit a dependence also on the relative velocity $\mathbf{v}_n - \mathbf{v}_s$ between the normal and the superfluid velocities.

At $T = 0$ where $n_n = 0$, the entropy identically vanishes and the Euler equation (1.3), thanks to the Gibbs-Duhem relation, coincides with equation (1.1). The two-fluid hydrodynamic equations (1.1-1.4) then reduce to the equation of continuity and to the equation for the irrotational superfluid

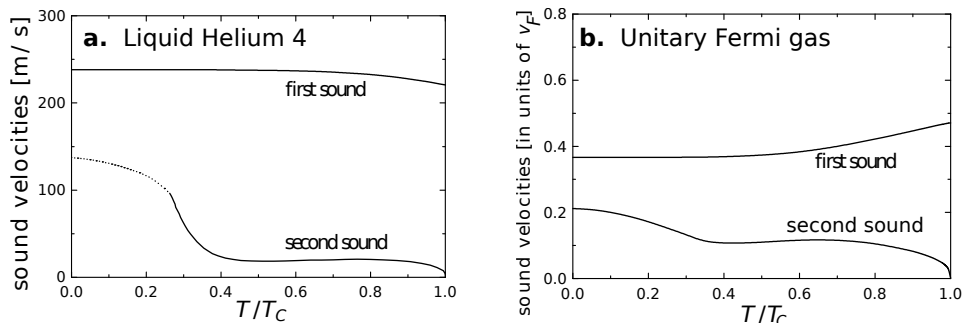


Figure 1.1 (a) Experimental values of first and second sound speeds in superfluid ^4He . Dots correspond to the theoretical calculation accounting for the contribution of the phonon-roton excitations to the thermodynamic functions. (b) Two-fluid sound speeds in a uniform Fermi gas at unitarity calculated using the NSR thermodynamic functions. From [57]

velocity. Viceversa, for temperatures larger than the critical value, where the superfluid density vanishes and the equation for the superfluid velocity can be ignored, the other three equations reduce to the classical equations of dissipationless hydrodynamics.

Let us for the moment ignore the external potential V_{ext} . By looking for plane wave solutions varying in space and time like $e^{-i\omega(t-x/c)}$, after a lengthy but straightforward calculation one obtains (see, for example, [49]), the Landau's equation for the sound velocity [31].

$$c^4 - \left[\frac{1}{mn\kappa_s} + \frac{n_s T \bar{s}^2}{mn_n \bar{c}_v} \right] c^2 + \frac{n_s T \bar{s}^2}{mn_n \bar{c}_v} \frac{1}{mn\kappa_T} = 0, \quad (1.5)$$

where $\bar{c}_v = T(\partial\bar{s}/\partial T)_n$ is the specific heat at constant volume per particle, $\kappa_s = (\partial n/\partial P)_{\bar{s}}/n$ and $\kappa_T = (\partial n/\partial P)_T/n$ are, respectively, the adiabatic and isothermal compressibilities while $\bar{s} = s/n$ is the entropy per particle.

If $n_s \neq 0$ equation (1.5) gives rise to two distinct sound velocities, known as first and second sound. This is the consequence of the fact that in a superfluid there are two degrees of freedom associated with the normal and superfluid components. The existence of two types of sound waves in a Bose-Einstein condensed system was first noted by Tisza [58]. The second sound velocity was measured in superfluid ^4He by Peshkov [46]. The values of the two sound velocities, measured in superfluid ^4He , are reported in Fig. 1.1(a) as a function of T .

The knowledge of the two sound velocities can be used to evaluate the density strengths associated with the corresponding modes and the consequent possibility of exciting them with a density probe. For example, using

a sudden laser perturbation, one excites both first and second sound with a relative weight given by the relative contribution of the two modes to the inverse energy weighted moment

$$\int_{-\infty}^{\infty} d\omega \frac{1}{\omega} S(\mathbf{q}, \omega) = \frac{1}{2} n \kappa_T \quad (1.6)$$

also known as the compressibility sum rule ([49] §7), fixed by the isothermal compressibility and here derived in the limit of small momentum transfer \mathbf{q} . In Eq. (1.6), $S(\mathbf{q}, \omega)$ is the dynamical structure factor with momentum \mathbf{q} and frequency ω . Taking into account the fact that at small wave vectors not only the inverse energy weighted sum rule, but also the energy weighted moment $\int_{-\infty}^{\infty} \omega S(\mathbf{q}, \omega) = q^2/2m$, known as f -sum rule, is exhausted by the two sound modes [48], one straightforwardly finds that the relative contributions to the compressibility sum rule (1.6) from each sound are given by [25]

$$W_1 \equiv \frac{1 - mn\kappa_T c_2^2}{2m(c_1^2 - c_2^2)}, \quad W_2 \equiv \frac{mn\kappa_T c_1^2 - 1}{2m(c_1^2 - c_2^2)}. \quad (1.7)$$

The Landau's equation (1.5) is easily solved as $T \rightarrow T_c$, i.e. close to the transition temperature where $\rho_s \rightarrow 0$. In this case the upper (first sound) and lower (second sound) solutions are given by

$$c_1^2 = \frac{1}{mn\kappa_s} = \frac{1}{m} \left(\frac{\partial P}{\partial n} \right)_s, \quad c_2^2 = \frac{n_s T \bar{s}^2}{mn_n \bar{c}_p}. \quad (1.8)$$

The first sound velocity is given by the isoentropic value and exhibits a continuous transition to the usual sound velocity above T_c . The second sound velocity is instead fixed by the superfluid density and vanishes at the transition where $n_s = 0$ in 3D systems. In the above equation we have introduced the specific heat at constant pressure \bar{c}_p , related to \bar{c}_v by the thermodynamic relation $\bar{c}_p/\bar{c}_v = \kappa_T/\kappa_s$.

Results (1.8) hold also in the $T \rightarrow 0$ limit where one can set $\kappa_T = \kappa_{\bar{s}}$, $\kappa_T = \kappa_s$ and $\bar{c}_p = \bar{c}_v$. In this limit all the thermodynamic functions as well as the normal density ρ_n are fixed by the thermal excitation of phonons and one can easily prove that Eq. (1.8) yields result $c_2^2 = c_1^2/3$ for the second sound velocity.

For systems characterized by a small thermal expansion coefficient $\alpha = -(1/n)\partial n/\partial T|_P = (\kappa_T/\kappa_s - 1)/T$, and hence very close values of the isothermal and adiabatic compressibilities), Eq. (1.8) provides an excellent approximation to the second sound velocity in the entire superfluid region $0 < T < T_c$. More precisely, the applicability of results (1.8) requires the

condition

$$\frac{c_2^2}{c_1^2} \alpha T \ll 1. \quad (1.9)$$

Systems satisfying the condition (1.9) include not only the well celebrated superfluid ^4He but also the interacting Fermi gas at unitarity (see Section 4). Furthermore, since in these cases $c_1^2 \sim (mn\kappa_s)^{-1} \sim (mn\kappa_T)^{-1}$, the second sound contribution to the compressibility sum rule (1.6) is negligible and consequently second sound should be excited using a thermal rather than a density perturbation [34]. Equation (1.8) for c_2 points out explicitly the crucial role played by the superfluid density and was actually employed to determine the temperature dependence of the superfluid density in liquid ^4He in a wide interval of temperatures [13].

Equations (1.8) are instead inadequate to describe the sound velocities in dilute Bose gases at intermediate values of T , due to the high isothermal compressibility exhibited by these systems as we will discuss in Sections 3 and 5.

1.3 Second sound in weakly interacting 3D Bose gases

An important consequence of the high compressibility exhibited by weakly interacting Bose gases is the occurrence of a hybridization phenomenon between first and second sound. This phenomenon, first investigated in the seminal paper by Lee and Yang [33], and later discussed by Griffin and co-workers (see, for example, [63, 18, 25]) has been recently investigated in detail in [60] where a suitable perturbative approach has been developed to explore the behavior of second sound below and above the hybridization point. The mechanism of hybridization is caused by the tendency of the velocity of the two modes to cross at very low temperatures, of the order of the zero temperature value of the chemical potential $\mu(T=0) = gn$ where $g = 4\pi\hbar^2 a/m$ is the bosonic coupling constant. This phenomenon characterizes dilute Bose gases and is absent in strongly interacting superfluids. It is natural to call the upper and lower branches as first and second sounds, respectively. For temperatures below the hybridization point the velocity of the upper branch approaches the Bogoliubov value $c_B = \sqrt{gn/m}$, while the lower branch approaches the Landau's result $c_2 = c_B/\sqrt{3}$. Above the hybridization point the role of first and second sound is inverted, in the sense that the lower (second sound) branch is essentially an oscillation of the superfluid density which practically coincides with the condensate density $n_0(T)$.

For temperatures higher than the hybridization temperature ($k_B T \gg gn$) a useful expression for the second sound velocity is obtained by evaluating all the quantities entering the quartic equation (1.5), except the isothermal compressibility and the superfluid density, using the ideal Bose gas model. One can actually show that the adiabatic compressibility, the specific heat at constant volume and the entropy density of a weakly interacting Bose gas deviate very little from the ideal Bose gas predictions in a wide interval of temperatures above the hybridization point. This simplifies significantly the solution of Equation (1.5). In fact in the ideal Bose gas model one finds:

$$\frac{1}{mn\kappa_s} + \frac{n_s T \bar{s}^2}{mn_n \bar{c}_v} = \frac{n T \bar{s}^2}{mn_n \bar{c}_v} \quad (1.10)$$

for the coefficient of the c^2 term. It is now easy to derive the two solutions satisfying the condition $c_1 \gg c_2$. To obtain the larger velocity c_1 one can neglect the last term in (1.5). Using the thermodynamic relations of the ideal Bose gas model and identifying the normal density with the thermal density ($n_T = n - n_0$) one obtains the prediction (here and in the following we take the Boltzmann constant $k_B = 1$)

$$c_1^2 = \frac{5}{3} \frac{g_{5/2}}{g_{3/2}} \frac{T}{m} \quad (1.11)$$

for the first sound velocity [33], where $g_{5/2}$ and $g_{3/2}$ are integrals of the Bose distribution function (see, for example, [49] §3.2). To calculate c_2 we must instead neglect the c^4 term in (1.5) and using result (1.10) one finds the useful result

$$c_2^2 = \frac{n_s}{n} \frac{1}{mn\kappa_T} \quad (1.12)$$

revealing that the superfluid density and the isothermal compressibility are the crucial parameters determining the value of the second sound velocity of weakly-interacting Bose gases for $T \gg gn$. Furthermore in a weakly interacting 3D Bose gas one can safely identify (except close to T_c) the inverse isothermal compressibility with its $T = 0$ value $(n\kappa_T)^{-1} = gn$ yielding the simple expression

$$c_2^2 = \frac{gn_s(T)}{m} \quad (1.13)$$

for the second sound velocity, revealing that second sound can be regarded, in this temperature range, as a finite temperature generalization of the Bogoliubov sound mode propagating at $T = 0$ at the velocity $\sqrt{gn/m}$ (at $T = 0$ one has $n_s = n$). Since in a weakly interacting 3D Bose gas the superfluid density can be safely approximated with the condensate density

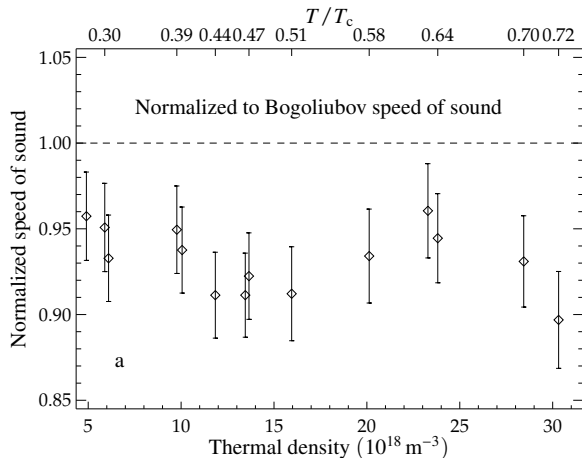


Figure 1.2 Speed of sound as a function of the thermal density. The upper axis gives the reduced temperature T/T_c for the corresponding data point. The speed of sound is normalized to the Bogoliubov sound velocity $\sqrt{gn_0(T)}/2m$ based on the central BEC density. From [38].

($n_s(T) = n_0(T)$) the above result also permits to understand that in the same regime of temperatures second sound corresponds to an oscillation of the condensate which can be easily excited through a density perturbation of the gas and subsequently imaged. In Fig. 1.2 we report the sound velocity measured in the experiment of [38], where a density perturbation was applied to a Bose gas confined in a highly elongated trap. Due to the harmonic radial confinement the density n entering the Bogoliubov formula should be actually replaced by $n/2$ where n is the central axial density [62] (a similar renormalization is expected to occur for the superfluid density and the condensate density at finite temperature). The good agreement between the measured sound velocity and the Bogoliubov value $\sqrt{gn_0(T)}/2m$, with the condensate fraction measured at the same value of T , permits to conclude that the sound excitation investigated in [38] actually corresponds to the second sound mode described above. The remaining small deviations are likely due to the approximations made to derive result (1.13) and to the identification $n_s = n_0$.

In order to explore the behavior of the sound velocities in the whole range of temperatures, including the hybridization region at low T , a more accurate knowledge of the thermodynamic functions entering the two-fluid hydrodynamic equations is needed. At low temperature ($T \ll T_c$) one can use Bogoliubov theory where the elementary excitations of the gas, whose dispersion is given by the Bogoliubov law $\varepsilon(\mathbf{p}) = \sqrt{(p^2/2m)(p^2/2m + 2gn)}$ are

thermally excited according to the bosonic rule $N_{\mathbf{p}}(\varepsilon) = (e^{\varepsilon(\mathbf{p})/kT} - 1)^{-1}$. Bogoliubov theory fails at temperatures of the order of the critical temperature where a more reliable approach is provided by the perturbation theory developed in Ref. [10] based on the Beliaev diagrammatic technique at finite temperature [2]. In this latter approach thermal effects in the Bogoliubov excitation spectrum are accounted for through a self-consistent procedure. At low temperatures this approach coincides with Bogoliubov theory, except for temperatures smaller than $(na^3)^{1/4}gn$, *i.e.* at temperatures much smaller than the hybridization point. At higher temperatures the theory of Ref. [10] turns out to be very accurate in dilute gases when compared with exact Monte-Carlo simulations. It follows that, at least for small values of the gas parameter na^3 , Bogoliubov theory and the diagrammatic approach of Ref. [10] match exactly in the hybridization region of temperatures $T \sim gn$ and that the thermodynamic behavior of the gas is consequently under control for all ranges of temperatures, both below and above gn .

The coefficients of the quartic equation (1.5) depend not only on the equilibrium thermodynamic functions, but also on the normal and superfluid densities. The normal density can be calculated using the Landau's prescription

$$mn_n = -\frac{1}{3} \int \frac{dN_{\mathbf{p}}(\varepsilon)}{d\varepsilon} p^2 \frac{d\mathbf{p}}{(2\pi\hbar)^3} \quad (1.14)$$

in terms of the elementary excitations of the gas. The Landau's prescription (1.14) ignores interaction effects among elementary excitations and in a dilute Bose gas is expected to be very accurate in the low temperature regime characterizing the hybridization point and to hold also at higher temperatures, except close to the critical point.

A peculiar property of the weakly-interacting Bose gas is that all the thermodynamic functions entering Eq. (1.5), as well as the normal density ρ_n , can be written in a rescaled form as a function of the reduced temperature $\tilde{t} \equiv T/gn$ and of the reduced chemical potential $\eta \equiv gn/T_C^0$ where

$$T_c^0 = \frac{2\pi\hbar^2}{m} \left(\frac{n}{\zeta(3/2)} \right)^{2/3} \quad (1.15)$$

is the critical temperature of the ideal Bose gas. In weakly-interacting Bose gases T_c^0 does not coincide with the actual critical temperature which contains a small correction fixed by the value of the gas parameter na^3 : $T_c = T_c^0(1 + \gamma(na^3)^{1/3})$ with $\gamma \sim 1.3$ [5, 4, 27]. The reduced chemical potential can be also expressed in terms of the gas parameter as $\eta = 2\zeta(3/2)^{2/3}(na^3)^{1/3}$.

Using Bogoliubov theory, the free energy $F = U - TS$ can be written as

$$\begin{aligned} \frac{F}{gnN} = & \frac{1}{2} \left[1 + \frac{128}{15\sqrt{\pi}} (na^3)^{1/2} \right] \\ & + \frac{2\tilde{t}}{\zeta(3/2)\sqrt{2\pi}} \eta^{3/2} \int_0^\infty \tilde{p}^2 \ln \left(1 - e^{-\frac{\tilde{t}}{2i}\sqrt{\tilde{p}^2+4}} \right) d\tilde{p}. \end{aligned} \quad (1.16)$$

where we have defined $\tilde{p} = p/\sqrt{mgn}$ and, for completeness, we have included the Lee-Huang-Yang correction to the $t = 0$ value of the free energy (term proportional to $(na^3)^{1/2}$). Starting from expression (1.16) for the free energy [60] all the thermodynamic functions entering Eq. (1.5) are easily calculated using standard thermodynamic relations. The normal density (1.14) is instead evaluated using Eq. (1.14), written in terms of the energy of the elementary excitations.

The idea now is to calculate the two solutions of Eq. (1.5) for a fixed value of \tilde{t} of the order of unity, taking the limit $\eta \rightarrow 0$. Physically this corresponds to considering very low temperatures (of the order of gn) and small values of the gas parameter na^3 . For example in the case of ^{87}Rb the value of the scattering length is $a = 100a_0$ (where a_0 is the Bohr radius) and typical values of the density correspond to $na^3 \sim 10^{-6}$. This yields $\eta \approx 0.04$.

Writing the solutions of Eq. (1.5) in terms of the $T = 0$ Bogoliubov velocity $c_B = \sqrt{gn/m}$, one finds that, as $\eta \rightarrow 0$, the two sound velocities only depend on the dimensionless parameter \tilde{t} and are given by

$$c_+^2 = c_B^2, \quad c_-^2 = c_B^2 f(\tilde{t}) \quad (1.17)$$

where $f(\tilde{t}) = \lim_{\eta \rightarrow 0} \frac{n}{n_n} \frac{T\bar{s}^2}{\bar{c}_v} \frac{1}{gn}$. One actually easily finds that $\bar{s} \propto \eta^{3/2}$, $\bar{c}_v \propto \eta^{3/2}$ and $n_n \propto \eta^{3/2}$ as $\eta \rightarrow 0$ and that f , in this limit, is consequently a function of \tilde{t} , independent of η . In the $\eta \rightarrow 0$ limit, the two velocities shown in Fig. 1.3(a) cross each other at the value $\tilde{t}_{\text{hyb}} \approx 0.6$. At lower temperatures c_-^2 approaches, as expected, the zero-temperature value $c_B^2/3$. By considering finite, although small, values of η , it is possible to show that, at the hybridization point, the two branches exhibit a gap proportional to $\eta^{3/4}$. The mechanism of hybridization, explicitly shown in the inset of Fig. 1.3(a), permits to identify an upper branch c_1 (which coincides with c_+ for $\tilde{t} < \tilde{t}_{\text{hyb}}$ and with c_- for $\tilde{t} > \tilde{t}_{\text{hyb}}$) called ‘‘first sound’’. The lower branch c_2 (called ‘‘second sound’’) instead coincides with c_- for $\tilde{t} < \tilde{t}_{\text{hyb}}$ and with c_+ for $\tilde{t} > \tilde{t}_{\text{hyb}}$.

The validity of Eqs. (1.17) is limited to very low temperatures where the thermal depletion of the condensate can be ignored and Bogoliubov theory

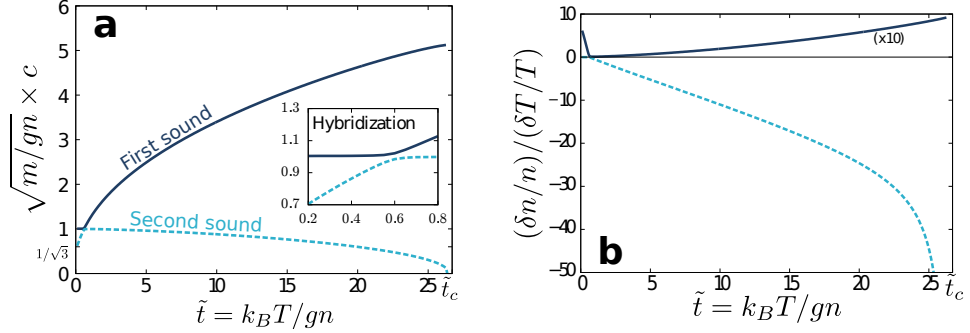


Figure 1.3 (a) Sound velocities (dashed light blue and solid dark blue lines) computed interpolating Bogoliubov theory and the diagrammatic approach of Ref. [10], over the whole range of temperatures $0 < \tilde{t} < \tilde{t}_c$. The inset shows the hybridization region. (b) Ratio $(\delta n/n)/(\delta T/T)$ for the lower branch (dashed light blue) and the upper branch (solid dark blue). The parameters are chosen as in Fig. 1.3(a). For both graphs, the gas parameter is chosen to be $na^3 = 10^{-6}$, and the critical point corresponds to $\tilde{t}_c = T_c/gn = 26.7$. From [60]

can be safely applied. When the temperature is comparable to the critical temperature T_c (corresponding to $\tilde{t}_c = 26.7$ in the case of Fig. 1.3(a), where we have chosen $\eta = 0.04$), Bogoliubov theory is no longer applicable. In fact at such temperatures the thermal depletion of the condensate becomes important and the Bogoliubov expression for the dispersion law is inadequate. The superfluid density fraction, calculated according to Eq. (1.14) with the $T = 0$ value of the Bogoliubov dispersion law, vanishes at $T \sim 1.2T_c$, well above the critical temperature, further revealing the inadequacy of the theory at high temperatures. As anticipated above a better approach to be used at temperatures of the order of the critical value is the diagrammatic approach of Ref. [10] whose predictions for the first and second sound velocities at temperatures higher than the hybridization temperature are reported in Fig. 1.3(a) and which properly interpolates with the predictions of Bogoliubov theory near the hybridization point.

In Fig. 1.3(b), we show the ratio $(\delta n/n)/(\delta T/T)$ between the relative density and temperature variations calculated for the first and second sound solutions of Eq. (1.5) as a function of temperature. This quantity represents an important characterization of the two branches. It is in fact well known that sound in an ideal classical gas is an adiabatic oscillation characterized by the value $3/2$ for the ratio $(\delta n/n)/(\delta T/T)$. For the upper solution of the hydrodynamic equations (first sound), this ratio is positive over the full range of temperatures below the transition and its value increases with

T , getting close to unity near the transition. The most important feature emerging from Fig. 1.3(b) is that the ratio between the relative density and temperature changes associated with the second sound solution, has an opposite sign and a much larger value in modulus, reflecting that second sound, for temperatures larger than the hybridization value is dominated by the fluctuations of the density, rather than by the ones of the temperature. This important feature is also revealed by the fact that, in the same range of temperatures, second sound practically exhausts the compressibility sum rule (1.6). This result can be easily understood from Eq. (1.7). In fact if $T \gg gn$ one has $mc_1^2 \gg (n\kappa_T)^{-1}$ and consequently $W_2 \gg W_1$. The fact that the compressibility sum rule (1.6) is strongly affected by second sound is a remarkable feature exhibited by the weakly-interacting Bose gas above the hybridization point which distinguishes in a profound way its behavior from the one of strongly interacting superfluids, like ^4He or the unitary Fermi gas, where the density fluctuations associated with second sound are very small.

From an experimental point of view the results discussed in this section, and in particular Fig. 1.3(b), reveal that, in dilute Bose gases, second sound is more easily accessible than first sound, being very sensitive to the coupling with the density probe. This is confirmed by the experimental identification of second sound in the experiment of Ref. [38]. It is finally worth noticing that the fact that second sound in a Bose gas can be easily excited through a density probe is not specific to the 3D case. Indeed, a similar behavior takes place also in 2D Bose gases [44] where its measurement could provide an efficient determination of the superfluid density, including its discontinuity at the Berezinski-Kosterlitz-Thouless transition (see Section 5).

1.4 Second sound in the unitary Fermi gas

The possibility of determining the temperature dependence of the superfluid density from the measurement of second sound represents a major challenge in the physics of interacting Fermi gases where, differently from the case of weakly interacting Bose gases discussed in the previous section, the superfluid density n_s cannot be identified with the condensate fraction and the theoretical determination of n_s at finite temperature remains a difficult problem from the many-body point of view. Recent progress in the experimental measurement of second sound of a Fermi gas [55] at unitarity has opened new perspectives in this direction and the first determination of the superfluid density in a Fermi superfluid.

First predictions for the temperature dependence of the first and sec-

ond sound velocities in the 3D unitary Fermi gas were obtained in [57] by calculating the thermodynamic functions entering the two-fluid Landau's hydrodynamic equation (1.5) using the Nozieres Schmitt-Rink (NSR) approach [42, 24] (see Fig. 1.1b). These result have provided a first estimate of the second sound velocity in this strongly interacting Fermi system. It is remarkable to see that the qualitative behavior of the second sound velocity of the unitary Fermi gas looks very similar to the one of superfluid ^4He (Fig. 1.1a).

In the following we will discuss the behavior of second sound developing the hydrodynamic formalism in the presence of a highly elongated trap, a configuration particularly suited to explore experimentally the propagation of sound. The effect of the radial confinement has the important consequence that the variations of the temperature $\delta T(z, t)$ and of the chemical potential $\delta\mu(z, T)$, as well as the axial velocity field $v_n^z(z, t)$ do not exhibit any dependence on the radial coordinate during the propagation of sound which can then be considered one dimensional in nature, although the local equilibrium properties of the system can be described using the 3D thermodynamic functions in the local density approximation. The validity of the 1D like assumption is ensured by collisional effects which restore a radial local thermodynamic equilibrium and requires the condition that the viscous penetration depth $\sqrt{\eta_s/mn_{n1}\omega}$ be larger than the radial size of the system. Here n_{n1} is the 1D normal density, obtained by radial integration of the normal density, η_s is the shear viscosity and ω is the frequency of the sound wave. In terms of the radial trapping frequency ω_\perp the condition can be written in the form $\omega \ll \omega_\perp^2 \tau$ where τ is a typical collisional time here assumed, for simplicity, to characterize both the effects of viscosity and thermal conductivity. The condition of radial local thermodynamic equilibrium would have a dramatic consequence in the presence of a tube geometry with hard walls. In fact in this case the viscosity effect near the wall would cause the vanishing of the normal velocity field, with the consequent blocking of the normal fluid. The resulting motion, involving only the superfluid fraction with the normal component at rest, is called fourth sound and was observed in liquid helium confined in narrow capillaries. In the presence of radial harmonic trapping this effect is absent and the normal component can propagate as well, allowing for the propagation of both first and second sound.

Under the above conditions of local radial equilibrium one can easily integrate radially the hydrodynamic equations (1.1-1.4) which then keep the

same form as for the 3D uniform gas [7]:

$$\partial_t n_1 + \partial_z j_z = 0 \quad (1.18)$$

$$m \partial_t v_s^z = -\partial_z (\mu_1(z) + V_{ext}(z)) \quad (1.19)$$

$$\partial_t s_1 + \partial_z (s_1 v_n^z) = 0 \quad (1.20)$$

$$\partial_t j_z = -\frac{\partial_z P_1}{m} - \frac{n}{m} \partial_z V_{ext}(z), \quad (1.21)$$

where $n_1(z, t) = \int dx dy n(\mathbf{r}, t)$, $s_1(z, t) = \int dx dy s(\mathbf{r}, t)$, and $P_1(z, t) = \int dx dy P(\mathbf{r}, t)$ are the radial integrals of their 3D counterparts, namely the particle density, the entropy density and the local pressure. The integration accounts for the inhomogeneity caused by the radial component of the trapping potential. In the above equations $j_z = n_{n1} v_n^z + n_{s1} v_s^z$ is the current density, $n_{s1} = \int dx dy n_s$ and $n_{n1} = \int dx dy n_n$ are the superfluid and the normal 1D densities respectively with $n_1 = n_{n1} + n_{s1}$, while v_s^z and v_n^z are the corresponding velocity fields. In eqn (1.19) $\mu_1(z, t) \equiv \mu(\mathbf{r}_\perp = 0, z, t)$ is the chemical potential calculated on the symmetry axis of the trapped gas. Its dependence on the 1D density and on the temperature is determined by the knowledge of the radial profile which can be calculated employing the equation of state of uniform matter in the local density approximation.

By setting the axial trapping $V_{ext}(z)$ equal to zero, which corresponds to considering a cylindrical geometry, we can look for sound wave solutions propagating with a phase factor of the form $e^{i(qz - \omega t)}$. One then derives the same Landau's equation (1.5) obtained in uniform matter, with the thermodynamic functions replaced by the corresponding 1D expressions, in particular the 1D entropy per particle is given by $\bar{s}_1 = s_1/n_1$ and the 1D specific heat at constant pressure by $\bar{c}_{p1} = T(\partial \bar{s}_1 / \partial T)_{p_1}$.

Also in the highly elongated 1D cigar configuration the Landau's equations admit two different solutions, corresponding to the first (c_1) and second (c_2) sound velocities. Simple results for the sound velocities are obtained under the condition (1.9), yielding the results

$$m c_1^2 = \left(\frac{\partial P_1}{\partial n_1} \right)_{\bar{s}_1} \quad m c_2^2 = T \frac{n_{s1} \bar{s}_1^2}{n_{n1} \bar{c}_{p1}} \quad (1.22)$$

for the first and second sound velocity, respectively.

Some comments are in order here: i) The assumption (1.9), yielding results (1.22) is well satisfied in strongly interacting superfluid Fermi gases in the whole temperature interval below T_c due to their small compressibility

(from this point of view the behavior of the solutions of the hydrodynamic equations deeply differ from the case of dilute Bose gases discussed in the previous Section). ii) The expression (1.22) for the second sound velocity contains the specific heat at constant pressure. This reflects the fact that second sound actually corresponds to a wave propagating at constant pressure rather than at constant density. This difference is very important from the experimental point of view. In fact, even a small value of the thermal expansion coefficient is crucial in order to give rise to measurable density fluctuations during the propagation of second sound [55]. iii) The thermodynamic ingredients P_1 , \bar{s}_1 and \bar{c}_{P1} are known with good precision at unitarity in a useful range of temperatures. They can be easily determined starting from the 3D thermodynamic relations holding for the uniform Fermi gas at unitarity.

In the following we will outline the calculation of the thermodynamic functions in the case of the unitary Fermi gas [23]. At unitarity, the only length scales for uniform configurations are the interparticle distance, fixed by the density of the gas, and the thermal wavelength $\lambda_T = \sqrt{2\pi\hbar^2/mT}$, fixed by the temperature. Correspondingly, the energy scales are now the temperature and the Fermi temperature

$$T_F = \frac{\hbar^2}{2m}(3\pi^2n)^{2/3} \quad (1.23)$$

or, in alternative, the chemical potential μ . It follows that at unitarity all the thermodynamic functions can be expressed [21] in terms of a universal function $f_p(x)$ depending on the dimensionless parameter $x \equiv \mu/T$. This function can be defined in terms of the pressure and the density of the gas, according to the relationships

$$P \frac{\lambda_T^3}{T} = f_p(x), \quad n\lambda_T^3 = f'_p(x) \equiv f_n(x). \quad (1.24)$$

From Eq. (1.24) for the density one derives the useful relationship $T/T_F = 4\pi/[3\pi^2 f_n(x)]^{2/3}$ for the ratio between the temperature and the Fermi temperature in terms of the ratio x .

In terms of f_n and f_p we can calculate all the thermodynamic functions of the unitary Fermi gas. For example, using the thermodynamic relation $s/n = -(\partial\mu/\partial T)_P$, we find the result $\bar{s} = s/n = (5/2)f_p/f_n - x$ for the entropy per unit mass. It is worth noting that the above equations for the thermodynamic functions of the unitary Fermi gas are formally identical to the ones of the ideal Fermi gas, the dimensionless functions f_p and f_n replacing, apart from a factor 2 caused by spin degeneracy, the usual $F_{5/2}$ and $F_{3/2}$ Fermi integrals (see [49], §16.1). Since the entropy \bar{s} depends only

on the dimensionless parameter x , from Eqs. (1.24) one finds that during an adiabatic transformation the quantity $P/n^{5/3}$ remains constant, which is the same condition characterizing a non-interacting monoatomic gas.

The scaling function $f_p(x)$ (and hence its derivative $f_n(x)$) can be determined through microscopic many-body calculations or extracted directly from experiments carried out in trapped configurations from which it is possible to build the equation of state of uniform matter [30]. The experimental analysis of the thermodynamic functions (in particular the isothermal compressibility and the specific heat) has allowed for the identification of the critical temperature associated with the superfluid phase transition for which the authors of [30] have found the result

$$T_c = 0.167T_F, \quad (1.25)$$

in agreement with the most recent reliable theoretical calculations, based on Quantum Monte Carlo [9, 17] and diagrammatic [20] techniques. The value of T_c corresponds to $x_c = \mu_c/T_c = 2.48$.

Using the local density approximation along the radial direction, which is obtained by replacing the chemical potential with $\mu = \mu_0 - (1/2)m\omega_\perp^2 r_\perp^2$, and integrating the thermodynamic functions P , n and s along the radial directions, it is possible to construct the corresponding 1D thermodynamic functions in terms of the 1D chemical potential $\mu_1 = x_1 T$, which are needed to calculate the ingredients entering the Landau's equation for the 1D two sound velocities. One finds [23]

$$P_1 = \frac{2\pi}{m\omega_\perp^2} \frac{T^2}{\lambda_T^3} f_q(x_1), \quad n_1(x_1, T) = \frac{2\pi}{m\omega_\perp^2} \frac{T}{\lambda_T^3} f_p(x_1), \quad (1.26)$$

with $f_q = \int_{-\infty}^x dx' f_p(x')$, allowing for the determination of the various thermodynamic functions. In particular the 1D entropy per unit mass takes the form $\bar{s}_1 = s_1/n_1 = (7/2)f_q(x_1) - x_1 f_p(x_1)$. From the above equations it follows immediately that $(\partial P_1/\partial n_1)_{\bar{s}_1} = (7/5)P_1/n_1$ which differs from the adiabatic result $(\partial P/\partial n)_{\bar{s}} = (5/3)P/n$ holding in the 3D case. Using Equation (1.22) one then predicts the result

$$mc_1^2 = \frac{7}{5} \frac{P_1}{n_1} \quad (1.27)$$

for the first sound velocity in good agreement with the experimental findings (see Figure 1.4).

Since the temperature dependence of the superfluid density is not known theoretically in the unitary Fermi gas with sufficient accuracy, for the discussion of second sound we will follow a different strategy: we will employ

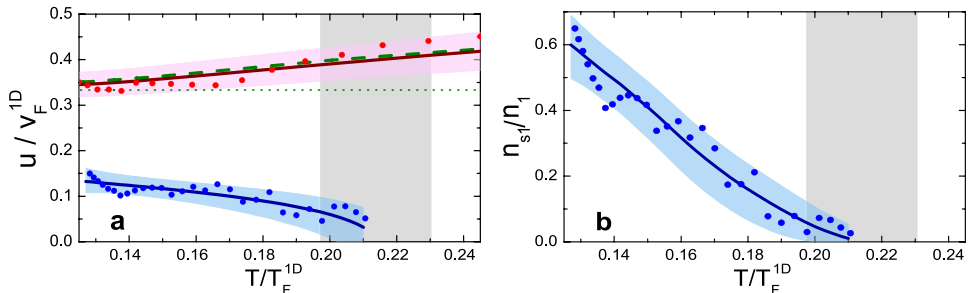


Figure 1.4 **a**, Speeds of first and second sound of the unitary Fermi gas in a highly elongated trap, normalized to the local Fermi speed and plotted as a function of the reduced temperature. The dashed curve is a prediction based on Eq. 1.27 and the EOS from ref. [30]. The dotted horizontal line is the zero-temperature limit for the speed of first sound. **b**, Temperature dependence of the 1D superfluid fraction n_{s1}/n_1 . From [55]

the measured value of the 1D second sound velocity (see discussion below) to extract $n_{s1}(T)$ from Eq. (1.22). By the way, in the low temperature regime, the calculation of the thermodynamic functions in the highly elongated geometry predicts $c_2 \propto \sqrt{T} \rightarrow 0$, differently from the uniform 3D case where $c_2 \rightarrow c_1/\sqrt{3}$. Thus the 1D second sound velocity c_2 tends to zero both as $T \rightarrow T_c$ and $T \rightarrow 0$. As a consequence, in the cigar geometry, the condition (1.9) is rather well satisfied for all temperatures and Eq. (1.22) is expected to be particularly accurate.

Fig. 1.4 shows the measured sound velocities in the experiment of [55] carried out in a highly elongated Fermi gas at unitarity. The excitation of first and second sounds was obtained by generating, respectively, a sudden local perturbation of the density and of the temperature in the center of the trapped gas. Due to the finite, although small, value of the thermal expansion coefficient of the unitary Fermi gas also the thermal perturbation, generating the second sound wave, gives rise to a measurable density pulse. In this experiment both the first and second sound velocities were obtained by measuring, for a fixed value of T , the time dependence position of the density pulses generated by the perturbation. These measurements give access to the dependence of the sound velocity on the ratio T/T_F^{1D} where $T_F^{1D} = (15\pi/8)^{2/5}(\hbar\omega_\perp)^{4/5}(\hbar^2 n_1^2/2m)^{1/5}$ is a natural definition for Fermi temperature in 1D cylindrically trapped configurations [55, 23]. If n_1 is calculated for an ideal Fermi gas at zero temperature, T_F^{1D} coincides with the usual 3D definition of the Fermi temperature (1.23), with n calculated on the symmetry axis. In the presence of axial trapping the value of T/T_F^{1D} actually increases as one moves from the center, because of the density de-

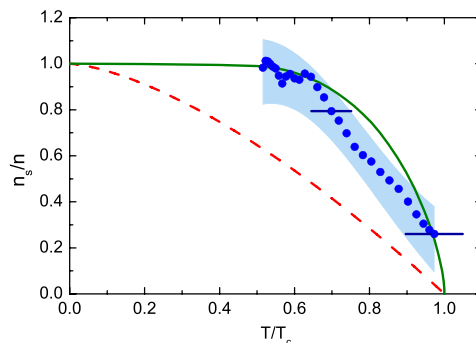


Figure 1.5 Superfluid fraction for the homogeneous case. The data points and the corresponding uncertainty range (shaded region) show the superfluid fraction for a uniform resonantly interacting Fermi gas versus T/T_c as reconstructed from its 1D counterpart in Fig. 1.4. The two horizontal error bars indicate the systematic uncertainties resulting from the limited knowledge of the critical temperature T_c . For comparison, we show the fraction for superfluid helium (solid line) as measured in Ref. [13] and the textbook expression $1 - (T/T_c)^{3/2}$ for the Bose-Einstein condensed fraction of the ideal Bose gas (dashed line). From [55]

crease, and eventually the density pulse reaches the transition point where the superfluid vanishes.

From the measurement of the temperature dependence of the 1D superfluid density and recalling the definition $n_{s1} = \int dx dy n_s$, one can reconstruct the 3D superfluid density n_s as a function of the ratio T/T_c [55], which is reported in Fig. 1.5. The measurement of n_s reported in the figure represents the first experimental determination of the temperature dependence of the superfluid density in a superfluid Fermi gas and could be used as a benchmark for future many-body calculations.

1.5 Second sound in the 2D Bose gas

Two dimensional superfluids differ in a profound way from their 3D counterparts. In fact, the Hohenberg-Mermin-Wagner theorem [22, 39] rules out the occurrence of long range order at finite temperature in 2D systems with continuous symmetry. Furthermore, the superfluid density approaches a finite value at the critical point of a 2D superfluid, known as Berezinskii-Kosterlitz-Thouless (BKT) transition [6, 28, 29, 41], rather than vanishing, as happens in 3D. With respect to the second order phase transitions characterizing the onset of superfluidity in 3D, the nature of the BKT phase transition is

deeply different, being associated with the emergence of a topological order, resulting from the pairing of vortices and antivortices. A peculiar property of these 2D systems is also the absence of discontinuities in the other thermodynamic functions at the critical temperature characterizing the transition to the superfluid phase. In order to identify the transition point, one has consequently to measure suitable transport properties. This is the case of the recent experiment of Ref. [14] on dilute two dimensional Bose gases where the superfluid critical velocity was measured in a useful range of temperatures, pointing up the occurrence of a sudden jump at a critical temperature when one enters the superfluid regime.

In this Section we discuss the behavior of both first and second sound in 2D superfluid gases, with particular emphasis on the discontinuity of their velocities at the critical point, caused by the jump of the superfluid density. Although the thermodynamic behavior of 2D dilute Bose gases is now well understood both theoretically [51, 50, 52] and experimentally [26, 61], the measurement of the superfluid density remains one of the main open issues. Besides the prospect of measuring the superfluid density, the measurement of second sound itself would be important because second sound has never been measured in any 2D system so far. In Helium films, the normal component of the liquid is in fact clamped to the substrate and cannot participate in the propagation of sound, only the superfluid being free to move (third sound). In Helium films, the value of n_s became accessible via third sound [54] and torsional oscillator measurements [8], confirming the superfluid jump at the transition. Since the trapping of dilute atomic gases is provided by smooth potentials, second sound is expected to propagate in these systems also in 2D and to be properly described by the two fluids Landau's hydrodynamic equations. Its propagation in dilute Bose gases exhibits very peculiar features as compared to less compressible fluids like helium or strongly interacting Fermi superfluid gases. In fact, in these latter systems second sound can be identified as an entropy oscillation and corresponds with good accuracy to an isobaric oscillation. This is not the case of dilute Bose gases which are highly compressible, giving rise to sizable coupling effects between density and entropy oscillations. Furthermore, with respect to the 3D case, in 2D, the superfluid density exhibits a jump at the transition and this shows up as a discontinuity of both first and second sound velocities [44] as we will discuss in the following.

We start our investigation by considering the Landau's two fluid hydrodynamic equations to describe the dynamics of the system in the superfluid phase of a 2D uniform configuration. The third direction is assumed to be blocked by a tight harmonic confinement, a condition well achieved in cur-

rent experiments. We will focus on the dilute 2D Bose gas, where all the thermodynamic ingredients can be written in terms of dimensionless functions [50, 26, 61]. These depend only on the variable $x \equiv \mu_2/T$ and on the 2D coupling constant $g_2 = (\hbar^2/m)\sqrt{8\pi}a/l$, where μ is the chemical potential, a is the three-dimensional scattering length, and l is the oscillator length in the confined direction. Here, we assume $l \gg a$ so that the interaction is momentum independent [47]. We introduce the dimensionless reduced pressure \mathcal{P} and the phase space density \mathcal{D} by

$$P_2\lambda_T^2/T \equiv \mathcal{P}(x, mg_2/\hbar^2), \quad n_2\lambda_T^2 \equiv \mathcal{D}(x, mg_2/\hbar^2), \quad (1.28)$$

where λ_T is the thermal de Broglie wavelength, P_2 and n_2 are the 2D pressure, and particle number density, respectively. The simple relation $\partial\mathcal{P}/\partial x = \mathcal{D}$ follows from thermodynamics. Starting from (1.28) one can evaluate the thermodynamic functions of the gas. In particular the entropy per unit mass, for a fixed value of g_2 , depends solely on the parameter x_2 : $\bar{s}_2 = s_2/n_2 = 2\mathcal{P}/\mathcal{D} - x_2$. The above equations reflect the universal nature of the thermodynamic behavior of the 2D Bose gas, for a fixed value of the coupling constant g_2 . The function \mathcal{D} has been numerically calculated for values of g_2 much smaller than \hbar^2/m in [50], and both \mathcal{P} and \mathcal{D} have been theoretically [52] and experimentally [26, 61] determined around the superfluid transition. The results available from different methods well agree with each other.

The superfluid density n_s cannot be calculated in terms of the universal functions introduced above, but can be nevertheless expressed in terms of another dimensionless function $\lambda_T^2 n_s \equiv \mathcal{D}_s(x, g_2)$, which is known close to the transition [50] as well as in the highly degenerate phonon regime (large and positive x). At the critical point one has $\mathcal{D}_s = 4$, which follows from the universal Nelson-Kosterlitz result $n_{2s} = 2mT_c/\pi\hbar^2$ [41], where T_c is the BKT transition temperature, providing an important relationship between the jump of the superfluid density at the transition and the value of the critical temperature.

The superfluid transition of a weakly interacting gas is predicted to take place at the value [51] $x_c = (mg_2/\pi\hbar^2) \log(\xi_\mu/g_2)$ with $\xi_\mu \approx 13.2\hbar^2/m$. For example, for $g_2 = 0.1\hbar^2/m$, a value relevant for the experiments of [61, 59, 14], the critical point corresponds to $x_c \approx 0.16$ or, in terms of the density, to $T_c = \{2\pi/\mathcal{D}(x_c)\}n_2/m \approx 0.76n/m$.

In Fig.1.6(a) we show the superfluid fraction n_{2s}/n_2 , calculated as a function of T/T_c for a fixed value of the total density, using the data from [50]. The figures correspond to the value $g_2 = 0.1\hbar^2/m$ and points out the large value of the superfluid fraction at the transition and the consequent jump.

As we will see below the jump of the superfluid density as well as the large value of the thermal expansion coefficient play an important role to characterize the solutions of the Landau's equation near the transition.

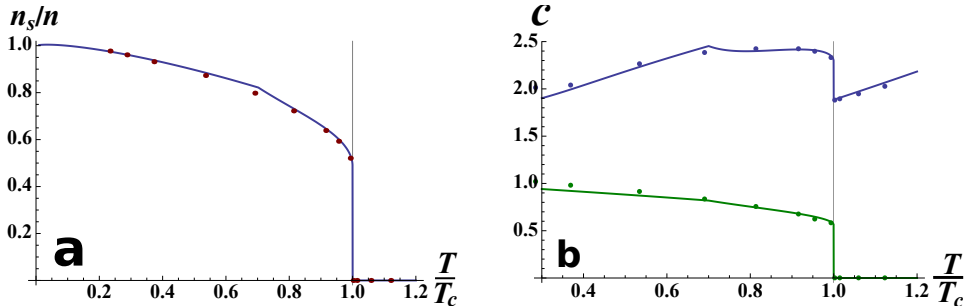


Figure 1.6 (a) Normalized superfluid density n_s/n for $mg_2/\hbar^2 = 0.1$. The line and the dots are calculated, respectively, from the approximate analytical and numerical results of [50]. Two analytical expressions valid at low and high temperatures are connected to give the curve, resulting in an unphysical kink at $T/T_c \sim 0.7$. (b) First and second sound velocities in units of the zero temperature Bogoliubov sound velocity $c_0 = \sqrt{g_2 n_2}/m$ with $mg_2/\hbar^2 = 0.1$, calculated by solving Eq. (1.5). From [44].

In Fig. 1.6(b) we show the values for the first and second sound velocities predicted by the solutions of Eq. (1.5). These values are expressed in units of the zero temperature value of the Bogoliubov sound velocity $c_0 \equiv \sqrt{g_2 n_2}/m$ and are calculated at fixed total density. The most remarkable feature emerging from the figure is the discontinuity exhibited by both the first and second sound velocities at the transition. Changing the value of the coupling constant g_2 does not affect the qualitative behavior of the sound velocities.

Using the parameters from the experiment of [14] carried out on a gas of ^{87}Rb atoms ($mg_2/\hbar^2 = 0.093$, $n_2 = 50/\mu\text{m}^2$), we predict the value $c_2 \approx 0.88$ mm/s for the second sound velocity at the transition. This value is close to the critical velocity observed in [14], thereby suggesting that the excitation of second sound is a possible mechanism for the onset of dissipation in this experiment.

Concerning the physical characterization of the two sounds it is worth recalling that in dilute Bose gases, first and second sound cannot be interpreted, respectively, as isoentropic and isobaric oscillations (see Eqs. (1.8)). In Section III we have already shown that in a weakly interacting 3D Bose gas, the second sound speed c_2 is instead well approximated by the expression (1.12) [49] rather than by Eq. (1.8), in the relevant region of temperatures $T \gg \mu$, where the isoentropic compressibility, the entropy, and the

specific heat at constant volume are very close to the predictions of the ideal Bose gas model. In two dimensions Eq. (1.12) describes exactly the second sound velocity the limit of small interactions ($g_2 \rightarrow 0$) [44]. For $g_2 = 0.1\hbar^2/m$ it is a good approximation (within $\sim 10\%$) to the second sound in the whole range of temperatures shown in Fig. 1.6(b). On the other hand, the first sound velocity around the transition can be estimated by solving Eq. (1.5) for small values of g_2 , which gives [44]

$$c_1^2 = c_{10}^2 + \alpha T c_{20}^2 \quad (1.29)$$

with c_{10}^2 and c_{20}^2 defined by Eqs. (1.8), with the thermodynamic quantities calculated in 2D. This result shows that both the nonzero thermal expansion coefficient α and the discontinuity in the superfluid density are responsible for the jump of the first sound velocity at the BKT transition.

One finds that in the whole interval of temperatures, second sound in the 2D Bose gas corresponds to an oscillation where mainly the superfluid is moving, the normal part remaining practically at rest. First sound, on the other hand, corresponds to an oscillation involving mainly the normal component, similarly to the case of 3D Bose gases (see Section II).

In order to measure first and second sound, a first important requirement is the reachability of the collisional hydrodynamic regime of fast collisions ($\omega\tau \ll 1$, where ω is the frequency of the sound and τ is a typical collisional time) in the normal part. This requirement is likely more problematic for first sound due to its higher velocity. The excitation of second sound should be more easily accessible not only because the velocity is lower but also because in dilute 2D Bose gases it can be naturally excited by density perturbations. For example, using a sudden laser perturbation, applied to the center of the trap, one excites both first and second sound with a relative weight given by Equation (1.7). Similarly to the 3D case also in the 2D Bose gas one finds that in the relevant temperature region $\mu \ll T < T_c$ one has $mc_1^2 \gg (n_2\kappa_T)^{-1}$ and hence $W_2 \gg W_1$. In this range of temperatures second sound hence provides most of the contribution to the compressibility sum rule thereby making its experimental excitation favorable through density perturbations. At lower temperatures, in the phonon regime, the situation is modified and a typical hybridization effect between the two sounds takes place [49], as discussed in the 3D case in Section II. As $T \rightarrow 0$, the thermodynamics is governed by phonons and the second sound velocity approaches the value $c_0/\sqrt{2}$. Above T_c , the difference between the isentropic and isothermal compressibilities is instead responsible for the occurrence of a diffusive mode at low frequency, like in 3D gases [25].

Typically, in experiments of dilute ultracold gases, atoms are harmonically

trapped also along the radial direction. In such systems, T/T_c depends on the local density and thus, by exciting the sound modes through perturbing the center of the trap and tracing the propagation of the modes, one could reveal the T/T_c dependence of the sound velocities, as observed in the case of three dimensional unitary Fermi gas [55] (see the previous Section).

1.6 Conclusions

We have presented an overview of recent theoretical and experimental advances in the study of the second sound velocity in ultracold atomic gases. Concerning possible perspectives and open problems in the future studies on second sound, we would like to mention the experimental determination of the second sound velocity in 2D quantum gases which would allow for the determination of the temperature dependence of the superfluid density in the presence of the Berzinski-Kosterlitz-Thouless transition. Other topics of great relevance, and so far unexplored either from the theoretical and experimental perspective, are the study of second sound in superfluid mixtures of Fermi and Bose gases [16] and the role of spin-orbit coupling, causing the breaking of Galilean invariance [65, 64, 45].

1.7 Acknowledgments

We would like to thank stimulating collaborations with Gianluca Bertaina, Rudolf Grimm, Yanhua Hou, Tomoki Ozawa, Leonid Sidorenkov and Meng Khoon Tey. We are also grateful to David Papoular for the final preparation of the paper. This work has been supported by ERC through the QGBE grant.

References

- [1] Abo-Shaeer, J. R., Raman, C., Vogels, J. M., and Ketterle, W. 2001. *Science*, **292**, 476.
- [2] Abrikosov, A. A., Gorkov, L. P., and Dzyaloshinskii, I. E. 1975. *Methods of Quantum Field Theory in Statistical Physics*. Dover.
- [3] Albiez, M., Gati, R., Fölling, J., Hunsmann, S., Cristiani, M., and Oberthaler, M. K. 2005. *Phys. Rev. Lett.*, **95**, 010402.
- [4] Arnold, P., and Moore, G. 2001. *Phys. Rev. Lett.*, **87**, 120401.
- [5] Baym, G., Blaizot, J.-P., Holzmann, M., Laloë, F., and Vautherin, D. 1999. *Phys. Rev. Lett.*, **83**, 1703.
- [6] Berezinskii, V. L. 1972. *Sov. Phys. JETP*, **34**, 610.

- [7] Bertaina, G., Pitaevskii, L., and Stringari, S. 2010. *Phys. Rev. Lett.*, **105**, 150402.
- [8] Bishop, D. J., and Reppy, J. D. 1978. *Phys. Rev. Lett.*, **40**, 1727.
- [9] Burovski, E., Prokof'ev, N., Svistunov, B., and Troyer, M. 2006. *Phys. Rev. Lett.*, **96**, 160402.
- [10] Capogrosso-Sansone, B., Giorgini, S., Pilati, S., Pollet, L., Prokof'ev, N., Svistunov, B., and Troyer, M. 2010. *New J. Physics*, **12**, 043010.
- [11] Chin, C., Bartenstein, M., Altmeyer, A., Riedl, S., Jochim, S., Hecker Denschlag, J., and Grimm, R. 2004. *Science*, **305**, 1128.
- [12] Coddington, I., Engels, P., Schweikhard, V., and Cornell, E. A. 2003. *Phys. Rev. Lett.*, **91**, 100402.
- [13] Dash, J. G., and Taylor, R. D. 1957. *Phys. Rev.*, **105**, 7.
- [14] Desbuquois, R., Chomaz, L., Yefsah, T., Léonard, J., Beugnon, J., Weitenberg, C., and Dalibard, J. 2012. *Nature Physics*, **8**, 645.
- [15] Donnelly, R. 2009. *Physics Today*, **62**(10), 34.
- [16] Ferrier-Barbut, I., Delehay, M., Laurent, S., Grier, A. T., Pierce, M., Rem, B. S., Chevy, F., and Salomon, C. 2014. *Science*, **345**, 1035.
- [17] Goulko, O., and Wingate, M. 2010. *Phys. Rev. A*, **82**, 053621.
- [18] Griffin, A., Nikuni, T., and Zaremba, E. 2009. *Bose-Condensed Gases at Finite Temperatures*. Cambridge University Press (New York).
- [19] Guéry-Odelin, D., and Stringari, S. 1999. *Phys. Rev. Lett.*, **83**, 4452.
- [20] Haussmann, R., Rantner, W., Cerrito, S., and Zwerger, W. 2007. *Phys. Rev. A*, **75**, 023610.
- [21] Ho, T.-L. 2004. *Phys. Rev. Lett.*, **92**, 090402.
- [22] Hohenberg, P. C. 1967. *Phys. Rev.*, **158**, 383.
- [23] Hou, Y.-H., Pitaevskii, L. P., and Stringari, S. 2013. *Phys. Rev. A*, **88**, 043630.
- [24] Hu, H., Liu, X.-J., and Drummond, P. D. 2006. *Phys. Rev. A*, **73**, 023617.
- [25] Hu, H., Taylor, E., Liu, X.-J., Stringari, S., and Griffin, A. 2010. *New J. Physics*, **12**, 043040.
- [26] Hung, C.-L., Zhang, X., Gemelke, N., and Chin, C. 2011. *Nature (London)*, **470**, 236.
- [27] Kashurnikov, V. A., Prokof'ev, N. V., and Svistunov, B. V. 2001. *Phys. Rev. Lett.*, **87**, 120402.
- [28] Kosterlitz, J. M., and Thouless, D. J. 1972. *J. Phys. C*, **5**, L124.
- [29] Kosterlitz, J. M., and Thouless, D. J. 1973. *J. Phys. C*, **6**, 1181.
- [30] Ku, M. J. H., Sommer, A. T., Cheuk, L. W., and Zwierlein, M. W. 2012. *Science*, **335**, 563.
- [31] Landau, L. D. 1941. *J. Phys. USSR*, **5**, 71.
- [32] Landau, L. D., and Lifshitz, E. M. 1987. *Fluid Mechanics*. Pergamon (Oxford).
- [33] Lee, T. D., and Yang, C. N. 1959. *Phys. Rev.*, **113**, 1406.
- [34] Lifshitz, E.M. 1944. *J. Phys. USSR*, **8**, 110.
- [35] Madison, K. W., Chevy, F., Wohlleben, W., and Dalibard, J. 2000. *Phys. Rev. Lett.*, **84**, 806.
- [36] Maragò, O. M., Hopkins, S. A., Arlt, J., Hodby, E., Hechenblaikner, G., and Foot, C. J. 2000. *Phys. Rev. Lett.*, **84**, 2056.
- [37] Matthews, M. R., Anderson, B. P., Haljan, P. C., Hall, D. S., Wieman, C. E., and Cornell, E. A. 1999. *Phys. Rev. Lett.*, **83**, 2498.
- [38] Meppelink, R., Koller, S. B., and van der Straten, P. 2009. *Phys. Rev. A*, **80**, 043605.
- [39] Mermin, N. D., and Wagner, H. 1966. *Phys. Rev. Lett.*, **17**, 1133.

- [40] Miller, D. E., Chin, J. K., Stan, C. A., Liu, Y., Setiawan, W., Sanner, C., and Ketterle, W. 2007. *Phys. Rev. Lett.*, **99**, 070402.
- [41] Nelson, D. R., and Kosterlitz, J. M. 1977. *Phys. Rev. Lett.*, **39**, 1201.
- [42] Nozières, P., and Schmitt-Rink, S. 1985. *J. Low Temp. Phys.*, **59**, 195.
- [43] Onofrio, R., Raman, C., Vogels, J. M., Abo-Shaeer, J. R., Chikkatur, A. P., and Ketterle, W. 2000. *Phys. Rev. Lett.*, **85**, 2228.
- [44] Ozawa, T., and Stringari, S. 2014. *Phys. Rev. Lett.*, **112**, 025302.
- [45] Ozawa, T., Pitaevskii, L. P., and Stringari, S. 2013. *Phys. Rev. A*, **87**, 063610.
- [46] Peshkov, V. P. 1946. *J. Phys. USSR*, **10**, 389.
- [47] Petrov, D. S., Holzmann, M., and Shlyapnikov, G. V. 2000. *Phys. Rev. Lett.*, **84**, 2551.
- [48] Pines, D., and Nozières, P. 1990. *Theory of Quantum Liquids*. Addison-Wesley (Redwood City).
- [49] Pitaevskii, L. P., and Stringari, S. 2016. *Bose-Einstein Condensation and Superfluidity*. Oxford University Press (New York).
- [50] Prokof'ev, N., and Svistunov, B. 2002. *Phys. Rev. A*, **66**, 043608.
- [51] Prokof'ev, N., Ruebenacker, O., and Svistunov, B. 2001. *Phys. Rev. Lett.*, **87**, 270402.
- [52] Rançon, A., and Dupuis, N. 2012. *Phys. Rev. A*, **85**, 063607.
- [53] Riedl, S., Sánchez Guajardo, E. R., Kohstall, C., Hecker Denschlag, J., and Grimm, R. 2011. *New J. Phys.*, **13**, 035003.
- [54] Rudnick, I. 1978. *Phys. Rev. Lett.*, **40**, 1454.
- [55] Sidorenkov, L. A., Tey, M. K., Grimm, R., Hou, Y.-H., Pitaevskii, L., and Stringari, S. 2013. *Nature (London)*, **498**, 78.
- [56] Stringari, S. 1996. *Phys. Rev. Lett.*, **77**, 2360.
- [57] Taylor, E., Hu, H., Liu, X.-J., Pitaevskii, L. P., Griffin, A., and Stringari, S. 2009. *Phys. Rev. A*, **80**, 053601.
- [58] Tisza, L. 1940. *J. Phys. Radium*, **1**, 164.
- [59] Tung, S., Lamporesi, G., Lobser, D., Xia, L., and Cornell, E. A. 2010. *Phys. Rev. Lett.*, **105**, 230408.
- [60] Verney, L., Pitaevskii, L., and Stringari, S. 2015. *arXiv:1506.06690*.
- [61] Yefsah, T., Desbuquois, R., Chomaz, L., Günther, K. J., and Dalibard, J. 2011. *Phys. Rev. Lett.*, **107**, 130401.
- [62] Zaremba, E. 1998. *Phys. Rev. A*, **57**, 518.
- [63] Zaremba, E., Nikuni, T., and Griffin, A. 1999. *J. Low Temp. Phys.*, **116**, 277.
- [64] Zheng, W., Yu, Z.-Q., Cui, X., and Zhai, H. 2013. *J. Phys. B*, **46**, 134007.
- [65] Zhu, Q., Zhang, C., and Wu, B. 2012. *Europhys. Lett.*, **100**, 50003.
- [66] Zwierlein, M. W., Abo-Shaeer, J. R., Schirotzek, A., Schunck, C. H., and Ketterle, W. 2005. *Nature*, **435**, 1047.